

Electronic Supplementary Information

RbB₃O₄F₂: A Rubidium Fluorooxoborate with Unprecedented

[B₃O₅F₂]³⁻ Functionalized Unit and Large Birefringence

Zixiu Lu,^{a,b} Fangfang Zhang,^{a,b,*} Abudukadi Tudi,^{a,b} Zhihua Yang^{a,b} and

Shilie Pan^{a,b,*}

^aCAS Key Laboratory of Functional Materials and Devices for Special Environments;
Xinjiang Technical Institute of Physics & Chemistry, CAS; Xinjiang Key Laboratory
of Electronic Information Materials and Devices, 40-1 South Beijing Road, Urumqi
830011, China.

^bCenter of Materials Science and Optoelectronics Engineering, University of Chinese
Academy of Sciences, Beijing 100049, China.

*Corresponding author: ffzhang@ms.xjb.ac.cn, slpan@ms.xjb.ac.cn.

Experimental Section

Crystal Growth. Single crystals of RbB₃O₄F₂ were grown by the high-temperature method in a closed system. A mixture of RbF (0.179 g, 1.713 mmol), Sr(BF₄)₂ (0.143 g, 0.858 mmol) and B₂O₃ (0.179 g, 2.571 mmol) were thoroughly ground, loaded into a tidy quartz tube (Φ 10 mm × 20 mm), which was washed with deionized water and dried in high-temperature to remove the inside impurities. The tube was flame-sealed under 10⁻³ Pa. The sample was gradually heated to 430 °C in 35 h and annealed at this temperature for 100 h, before cooled to 200 °C in 150 h. Many colorless sheet-like crystals with regular shapes were obtained.

Synthesis. Polycrystalline samples of RbB₃O₄F₂ can be synthesized by conventional solid-state methods based on the following reaction:



Stoichiometric amounts of RbF, NH₄BF₄ and H₃BO₃ were ground thoroughly and placed into a platinum crucible. The platinum crucible was heated to 230 °C for 10 h to decompose NH₃, BF₃ and H₂O, and then the temperature was raised to 350 °C and held for 5 days with several intermittent grindings. The phase purity of RbB₃O₄F₂ was confirmed by powder X-ray diffraction (XRD) pattern.

Single-Crystal XRD. Several fragments of a large crystal were first inspected using a polarizing microscope to exclude twinned crystals, and a suitable plate crystal was selected and mounted on a glass fiber with epoxy for the structure for the X-ray diffraction study. Single-crystal XRD data were recorded on a Bruker SMART APEX II diffractometer equipped with a 4K CCD area detector using monochromatic Mo-K α radiation ($\lambda = 0.71073 \text{ \AA}$). Data integration and absorption corrections were carried out using the Bruker *SAINt* program. The crystal structures were settled by the direct method with the SHELX-97 program package. The structure was solved using the

Intrinsic Phasing method provided by the ShelXT structure solution program and refined using the ShelXL least-squares refinement package. The structures were verified by using the ADDSYM algorithm from the program PLATON with no higher symmetry discovered. Crystal data and structure refinement information are summarized in Table S1 in the Electronic Supporting Information (ESI[†]). The final refined atomic positions and isotropic thermal parameters are given in Table S2 in the ESI[†]. Selected bond distances and bond angles are listed in Table S3 in the ESI[†].

Powder XRD. Powder XRD data were collected at room temperature with a Bruker D2 PHASER diffractometer equipped with Cu K α radiation ($\lambda = 1.5418 \text{ \AA}$) at room temperature. Data were collected in the angular (2θ) range of 10–60° with a scan step width of 0.02 ° and a fixed counting time of 1 s.

Elemental Analysis. Elemental analysis was carried on the clean single crystal surface with the aid of a JMS-7610FPlus field emission scanning electron microscope equipped with an Oxford X-MasN energy dispersive X-ray (EDX) detector with a 20 mm² window, operated with an accelerating voltage of 20 kV and a working distance of 10 mm.

Infrared Spectroscopy. The infrared spectra were recorded with a Shimadzu IR Affinity-1 Fourier transform infrared spectrometer in the range of 400 - 4000 cm⁻¹ with a resolution of 4 cm⁻¹. Pellets for measurement were prepared by pressing a thoroughly ground mixture of the target compounds and KBr with mass ratio about 1:100

UV-vis-NIR Diffuse Reflectance Spectroscopy.

The optical diffuse reflectance spectrum of powder sample was measured in the wavelength range from 190 to 2600 nm at room temperature using a SolidSpec-3700DUV spectrophotometer equipped with an integrating sphere attachment and

tetrafluoroethylene as a reference.

Computational Methods.

The electronic structures of title compounds were calculated using the CASTEP package with the norm-conserving pseudopotentials (NCP).¹ The exchange-correlation functional was Perdew-Burke-Emzerhof (PBE) functional² within the generalized gradient approximation (GGA)³. For the material, the plane-wave energy cutoff was set at 940.0 eV, and the k-point separation was set as 0.04 Å⁻¹ in the Brillouin zone. The empty bands were set as 3 times of valence bands in the calculation to ensure the convergence of optical properties. It is well known that GGA usually underestimates the bandgap owing to the discontinuity of exchange-correlation energy functional. Therefore, the HSE06 hybrid functional,⁴ was adopted to provide more accurate band gap values. The exchanged Coulomb potential in the screened hybrid functional of Heyd, Scuseria, and Ernzerhof (HSE) includes two parts, short-range (SR) and long-range (LR), and the screening parameter ω defines the separation range. **The HSE XC functional energy is calculated as follows,**

$$E_{xc}^{\text{HSE}} = aE_x^{\text{HF,SR}}(\omega) + (1-a)E_x^{\text{PBE,SR}}(\omega) + E_x^{\text{PBE,LR}}(\omega) + E_c^{\text{PBE}}$$

where the $E_x^{\text{HF,SR}}$, $E_x^{\text{PBE,SR}}$, $E_x^{\text{PBE,LR}}$, and E_c^{PBE} represent short-range Hartree-Fock exchange, short-range PBE exchange, long-range PBE exchange, and PBE correlation energy, respectively. In HSE06, the parameters are suggested as $a = 0.25$ and $\omega = 0.11 \text{ bohr}^{-1}$. Because GGA gives a better description of optical properties, scissors operators 1.20 eV for RbB₃O₄F₂ were used to shift the conduction bands to agree with the bandgap values of HSE06. The linear optical properties (e.g., refractive index) were obtained using the real part of the dielectric function, $\epsilon(\omega) = \epsilon_1(\omega) + i\epsilon_2(\omega)$. The optimized valence electronic configurations for ultra-soft pseudopotentials are as follows: Rb: 5s¹, B: 2s²2p¹, O: 2s²2p⁴ and F: 2s²2p⁵. The Broyden-Fletcher-Goldfarb-Shanno (BFGS) minimization technique⁵ was employed for geometry optimization. All forces on the atoms were converged to less than 0.01 eV·Å⁻¹, the maximum ionic

displacement was within 5×10^{-4} Å and the energy change was less than 5.0×10^{-7} eV. The response electron distribution anisotropy (REDA)⁶ approximation was introduced to analyze the relationship between optical anisotropy and distribution of bonding electrons in RbB₃O₄F₂. The birefringence can be estimated by the anisotropic valence bond of anionic groups as:

$$\Delta n = \frac{\Re \sum_g [N_c Z_a \Delta \rho^b]_g}{2n_1 E_0}$$

REDA index $\zeta = \sum_g [N_c Z_a \Delta \rho^b / (n_1 E_0)]_g$ of the anionic groups contained in the same crystal.

Where N_c is the coordination number of the nearest neighbor cations to the anion, E_0 is the optical bandgap, $\Delta \rho^b = \rho_{\max}^b - \rho_{\min}^b$, ρ_{\max}^b and ρ_{\min}^b are the maximum and minimum of the covalent electron density of the covalent bond on the optical principal axes of a crystal, and n_1 is the minimum refractive index.

Table S1. Crystal data and structure refinement for RbB₃O₄F₂.

Empirical formula	RbB ₃ O ₄ F ₂
Temperature	293(2) K
Crystal system, space group	Monoclinic, <i>P2₁/c</i>
Unit cell dimensions	$a = 4.698(10)$ Å $b = 17.770(10)$ Å, $\beta = 118.95^\circ$ $c = 7.328(12)$ Å
Volume	535.3(15) Å ³
Z, Calculated density	4, 2.728 g·cm ⁻³
Absorption coefficient	9.230 mm ⁻¹
<i>F</i> (000)	408
Theta range for data collection	2.292 to 25.242 °
Limiting indices	$-6 \leq h \leq 5, -22 \leq k \leq 14, -9 \leq l \leq 9$
Reflections collected / unique	3167 / 1191 [$R(\text{int}) = 0.0725$]
Completeness to theta = 25.242 °	99.9 %
Data / restraints / parameters	1191 / 0 / 92
Goodness-of-fit on <i>F</i> ²	1.007
Final <i>R</i> indices [$F_o^2 > 2\sigma(F_o^2)$] ^[a]	$R_1 = 0.0524, wR_2 = 0.0907$
<i>R</i> indices (all data) ^[a]	$R_1 = 0.0924, wR_2 = 0.1037$
Largest diff. peak and hole	0.768 and -0.721 e·Å ⁻³

^[a] $R_1 = \Sigma|F_o| - |F| / \Sigma|F_o|$ and $wR_2 = [\sum w(F_o^2 - F_c^2)^2 / \sum wF_o^4]^{1/2}$ for $F_o^2 > 2\sigma(F_o^2)$

Table S2. Atomic coordinates and equivalent isotropic displacement parameter for RbB₃O₄F₂.

Atoms	<i>x</i>	<i>y</i>	<i>z</i>	$U_{(eq)}^*$
Rb1	9361(2)	744(1)	7646(1)	34(1)
B1	11247(19)	1902(4)	4146(13)	25(2)
B2	6098(19)	2351(5)	1606(12)	26(2)
B3	6809(19)	1012(4)	2214(13)	21(2)
O1	9385(11)	2480(3)	2941(7)	31(1)
O2	14414(10)	2001(2)	5699(7)	31(1)
O3	10004(11)	1198(2)	3959(7)	26(1)
O4	4777(10)	1662(3)	1320(7)	31(1)
F1	7257(9)	652(2)	665(6)	38(1)
F2	5327(9)	491(2)	2915(6)	36(1)

$U_{(eq)}^*$ is defined as one-third of the trace of the orthogonalized U_{ij} tensor.

Table S3. Selected bond lengths [Å] and angles [deg] for RbB₃O₄F₂.

Rb1-F1 ^{#1}	2.831(5)	B1-O3	1.360(9)
Rb1-F1 ^{#2}	2.882(4)	B1-O1	1.361(8)
Rb1-F1 ^{#5}	3.277(8)	B1-O2	1.378(9)
Rb1-F2 ^{#3}	2.993(5)	B2-O4	1.343(9)
Rb1-F2	3.074(6)	B2-O2 ^{#7}	1.373(8)
Rb1-F2 ^{#2}	3.494(6)	B2-O1	1.390(9)
Rb1-F2 ^{#5}	3.534(6)	B3-F2	1.398(8)
Rb1-O3	2.972(6)	B3-F1	1.405(9)
Rb1-O2 ^{#4}	3.035(5)	B3-O4	1.438(8)
Rb1-O4 ^{#5}	3.123(5)	B3-O3	1.463(9)
Rb1-O1 ^{#6}	3.163(5)		
F1 ^{#1} -Rb1-F1 ^{#2}	86.74(14)	O4 ^{#5} -Rb1-F1 ^{#5}	42.30(11)
F1 ^{#1} -Rb1-O3	162.49(12)	O1 ^{#6} -Rb1-F1 ^{#5}	92.19(11)
F1 ^{#2} -Rb1-O3	110.28(13)	F1 ^{#1} -Rb1-F2 ^{#2}	126.53(12)
F1 ^{#1} -Rb1-F2 ^{#3}	63.45(13)	F1 ^{#2} -Rb1-F2 ^{#2}	39.94(11)
F1 ^{#2} -Rb1-F2 ^{#3}	69.15(16)	O3-Rb1-F2 ^{#2}	70.77(12)
O3-Rb1-F2 ^{#3}	117.77(13)	F2 ^{#3} -Rb1-F2 ^{#2}	92.49(16)
F1 ^{#1} -Rb1-O2 ^{#4}	86.12(16)	O2 ^{#4} -Rb1-F2 ^{#2}	146.59(13)
F1 ^{#2} -Rb1-O2 ^{#4}	166.56(12)	F2-Rb1-F2 ^{#2}	82.01(14)
O3-Rb1-O2 ^{#4}	76.39(15)	O4 ^{#5} -Rb1-F2 ^{#2}	95.70(17)
F2 ^{#3} -Rb1-O2 ^{#4}	97.46(17)	O1 ^{#6} -Rb1-F2 ^{#2}	130.95(12)
F1 ^{#1} -Rb1-F2	127.94(17)	F1 ^{#5} -Rb1-F2 ^{#2}	53.72(13)
F1 ^{#2} -Rb1-F2	105.62(12)	F1 ^{#1} -Rb1-F2 ^{#5}	62.04(18)
O3-Rb1-F2	45.01(15)	F1 ^{#2} -Rb1-F2 ^{#5}	55.97(10)
F2 ^{#3} -Rb1-F2	74.14(13)	O3-Rb1-F2 ^{#5}	130.69(17)
O2 ^{#4} -Rb1-F2	70.35(12)	F2 ^{#3} -Rb1-F2 ^{#5}	101.45(12)
F1 ^{#1} -Rb1-O4 ^{#5}	78.66(19)	O2 ^{#4} -Rb2-F2 ^{#5}	128.97(12)
F1 ^{#2} -Rb1-O4 ^{#5}	91.69(14)	F2-Rb1-F2 ^{#5}	160.63(15)
O3-Rb1-O4 ^{#5}	104.07(17)	O4 ^{#5} -Rb1-F2 ^{#5}	40.55(11)
F2 ^{#3} -Rb1-O4 ^{#5}	137.71(14)	O1 ^{#6} -Rb1-F2 ^{#5}	94.45(11)
O2 ^{#4} -Rb1-O4 ^{#5}	98.04(14)	F1 ^{#5} -Rb1-F2 ^{#5}	38.39(9)
F2-Rb1-O4 ^{#5}	148.09(12)	F2 ^{#2} -Rb1-F2 ^{#5}	79.33(15)
F1 ^{#1} -Rb1-O1 ^{#6}	89.74(12)	O3-B1-O1	121.3(6)
F1 ^{#2} -Rb1-O1 ^{#6}	147.82(12)	O3-B1-O2	116.1(6)
O3-Rb1-O1 ^{#6}	78.03(13)	O1-B1-O2	122.5(7)
F2 ^{#3} -Rb1-O1 ^{#6}	135.98(13)	O4-B2-O2 ^{#7}	125.1(6)
O2 ^{#4} -Rb1-O1 ^{#6}	43.50(13)	O4-B2-O1	122.1(6)
F2-Rb1-O1 ^{#6}	101.70(12)	O2 ^{#7} -B2-O1	112.7(6)
O4 ^{#5} -Rb1-O1 ^{#6}	56.32(12)	F2-B3-F1	106.9(6)
F1 ^{#1} -Rb1-F1 ^{#5}	100.31(18)	F2-B3-O4	111.1(6)
F1 ^{#2} -Rb1-F1 ^{#5}	57.21(14)	F1-B3-O4	108.9(6)
O3-Rb1-F1 ^{#5}	92.70(16)	F2-B3-O3	108.1(6)

F2 ^{#3} -Rb1-F1 ^{#5}	125.00(14)	F1-B3-O3	108.5(6)
O2 ^{#4} -Rb1-F1 ^{#5}	135.48(12)	O4-B3-O3	113.0(6)
F2-Rb1-F1 ^{#5}	129.23(10)		

Symmetry transformations used to generate equivalent atoms:

```

#1  x, y, z+1   #2 -x+2, -y, -z+1   #3 -x+1, -y, -z+1   #4 x-1, y,
z   #5 x+1, y, z+1   #6 x, -y+1/2, z+1/2   #7 x-1, -y+1/2, z-1/2
#8 x, -y+1/2, z-1/2   #9 x-1, y, z-1   #10 x+1, -y+1/2, z+1/2
#11 x+1, y, z   #12 x, y, z-1

```

Table S4. The investigation of the reported inorganic fluorooxoborates.

Compounds	Space groups	FBB	Anionic framework	Birefringence (@1064 nm)		Bandgap(eV)		Refs
				Exp.	Cal.	Exp.	Cal.	
BaBO ₃ F	<i>Pnma</i>	BO ₂ F ₂	[BOF ₃] chain	—	—	—	7.01	7
BaB ₂ O ₃ F ₂	<i>P2</i> ₁	B ₂ O ₆ F	[B ₂ O ₃ F] layer	—	—	—	7.00	8
BiB ₂ O ₄ F	<i>P3</i> ₂	B ₂ O ₆ F	[B ₂ O ₄ F] chain	—	0.018	4.43	—	9
SnB ₂ O ₃ F ₂	<i>P3</i> ₁ <i>m</i>	B ₂ O ₅ F ₂	[B ₂ O ₃ F] layer	—	—	3.72	—	10
PbB ₂ O ₃ F ₂	<i>P3</i> ₁ <i>m</i>	B ₂ O ₅ F ₂	[B ₆ O ₁₂ F ₆] layer	—	—	5.10	—	10b
K _{0.42} Rb _{2.58} B ₃ O ₃ F ₆	<i>Pbcn</i>	B ₃ O ₃ F ₆	[B ₃ O ₃ F ₆] cluster	—	—	5.64	—	11
Li ₂ B ₃ O ₄ F ₃	<i>P2</i> ₁ <i>2</i> ₁ <i>2</i> ₁	B ₃ O ₅ F ₃	[B ₃ O ₄ F ₃] chain	—	0.05	—	8.43	12
Na ₃ B ₃ O ₃ F ₆	<i>C2/c</i>	B ₃ O ₃ F ₆	[B ₃ O ₃ F ₆] cluster	—	—	—	—	13
K ₃ B ₃ O ₃ F ₆	<i>P2</i> ₁ / <i>n</i>	B ₃ O ₃ F ₆	[B ₃ O ₃ F ₆] cluster	—	—	5.40	—	14
Cs _{1.29} Rb _{1.71} B ₃ O ₃ F ₆	<i>P2</i> ₁ / <i>c</i>	B ₃ O ₃ F ₆	B ₃ O ₃ F ₆ cluster	—	—	—	—	15
Na _{0.76} Rb _{2.24} B ₃ O ₃ F ₆	<i>P2</i> ₁ / <i>c</i>	B ₃ O ₃ F ₆	B ₃ O ₃ F ₆ cluster	—	—	—	—	15
K _{2.64} Cs _{0.36} B ₃ O ₃ F ₆	<i>P2</i> ₁ / <i>c</i>	B ₃ O ₃ F ₆	B ₃ O ₃ F ₆ cluster	—	—	—	—	15
K _{1.66} Rb _{1.34} B ₃ O ₃ F ₆	<i>P2</i> ₁ / <i>c</i>	B ₃ O ₃ F ₆	B ₃ O ₃ F ₆ cluster	—	—	—	—	15
KCs ₂ B ₃ O ₃ F ₆	<i>P2</i> ₁ / <i>c</i>	B ₃ O ₃ F ₆	B ₃ O ₃ F ₆ cluster	—	—	—	8.13	15
Rb ₃ B ₃ O ₃ F ₆	<i>Pbcn</i>	B ₃ O ₃ F ₆	B ₃ O ₃ F ₆ cluster	—	—	—	8.15	15
K ₂ RbB ₃ O ₃ F ₆	<i>P2</i> ₁ / <i>c</i>	B ₃ O ₃ F ₆	B ₃ O ₃ F ₆ cluster	—	—	—	—	15
NaB ₄ O ₆ F	<i>C2</i>	B ₄ O ₈ F	[B ₄ O ₆ F] layer	—	0.120	>6.89	7.57	16
RbB ₄ O ₆ F	<i>Pna</i> 2 ₁	B ₄ O ₈ F	[B ₄ O ₆ F] layer	—	0.102	>6.20	7.73	17
CsB ₄ O ₆ F	<i>Pna</i> 2 ₁	B ₄ O ₈ F	[B ₄ O ₆ F] layer	0.11	0.098	8.00	8.01	18
NH ₄ B ₄ O ₆ F	<i>Pna</i> 2 ₁	B ₄ O ₈ F	[B ₄ O ₆ F] layer	0.12	0.107	7.95	7.85	19
CaB ₄ O ₆ F ₂	<i>P</i> 1̄	B ₄ O ₈ F	[B ₄ O ₆ F ₂] layer	—	0.091	—	7.72	20
SrB ₄ O ₆ F ₂	<i>P</i> 1̄	B ₄ O ₈ F	[B ₄ O ₆ F ₂] layer	—	0.089	—	7.81	20
BaB ₄ O ₆ F ₂	<i>P2</i> ₁ / <i>n</i>	B ₄ O ₈ F	[B ₄ O ₆ F ₂] layer	—	0.085	—	7.74	20
KNiB ₄ O ₆ F ₃	<i>P2</i> ₁ / <i>c</i>	B ₄ O ₆ F ₄	[B ₃ O ₆ F ₃] layer	—	—	—	—	21
Ba(B ₂ OF ₃ (OH) ₂) ₂	<i>C2/m</i>	B ₂ OF ₃ (O)H ₂	[B ₂ OF ₃ (OH)] cluster	—	0.086	—	8.35	22
CaB ₅ O ₇ F ₃	<i>Cmc</i> 2 ₁	B ₅ O ₉ F ₃	[B ₅ O ₇ F ₃] layer	—	0.070	>6.89	8.75	23
SrB ₅ O ₇ F ₃	<i>Cmc</i> 2 ₁	B ₅ O ₉ F ₃	[B ₅ O ₇ F ₃] layer	—	0.077	>6.89	8.58	23b, 24
PbB ₅ O ₇ F ₃	<i>Cmc</i> 2 ₁	B ₅ O ₉ F ₃	[B ₅ O ₇ F ₃] layer	—	0.120	—	5.56	25
PbB ₅ O ₈ F	<i>Pbca</i>	B ₅ O ₁₀ F	[B ₅ O ₈ F ₃] network	—	0.069	—	—	26
BaB ₅ O ₈ F·xH ₂ O	<i>Pbca</i>	B ₅ O ₁₀ F	[B ₅ O ₈ F ₃] network	—	0.055	—	—	27
Li ₂ Na _{0.9} K _{0.1} B ₅ O ₈ F ₂	<i>Pbca</i>	B ₅ O ₁₀ F ₂	[B ₅ O ₈ F ₂] layer	—	—	—	—	28
LiB ₆ O ₉ F	<i>Pna</i> 2 ₁	B ₆ O ₁₁ F	[B ₆ O ₉ F] layer	—	0.040	—	8.37	29
Li ₂ B ₆ O ₉ F ₂	<i>Cc</i>	B ₆ O ₁₁ F ₂	[B ₆ O ₉ F ₂] network	—	0.070	>6.53	8.05	30
Na ₂ B ₆ O ₉ F ₂	<i>P2</i> ₁ / <i>c</i>	B ₆ O ₁₁ F ₂	[B ₆ O ₉ F ₂] layer	0.08	0.064	7.33	—	31
NaRbB ₆ O ₉ F ₂	<i>P2</i> ₁ / <i>n</i>	B ₆ O ₁₁ F ₂	[B ₆ O ₉ F ₂] layer	—	—	—	—	32
K ₃ B ₆ O ₉ F ₃	<i>P2</i> ₁ / <i>c</i>	B ₆ O ₁₁ F ₃	[B ₆ O ₉ F ₃] cluster	—	—	6.98	—	33

Na ₃ B ₇ O ₁₁ F ₂	<i>Pnma</i>	B ₇ O ₁₃ F ₂	[B ₇ O ₁₃ F ₂] network	—	—	6.20	7.69	34
BaB ₈ O ₁₈ F ₂	<i>R</i> $\bar{3}c$	B ₄ O ₈ F	[B ₆ O ₆ F ₂] layer	—	0.120	—	6.85	35
CsKB ₈ O ₁₂ F ₂	<i>P</i> 321	B ₄ O ₈ F	[B ₄ O ₆ F] layer	—	0.105	>6.20	7.76	18
CsRbB ₈ O ₁₂ F ₂	<i>P</i> $\bar{6}2c$	B ₄ O ₈ F	[B ₄ O ₆ F] layer	—	—	>6.20	—	18
Ba ₃ B ₁₀ O ₁₇ F ₂ ·0.1KF	<i>P</i> $\bar{1}$	B ₁₀ O ₂₂ F	[B ₁₀ O ₁₆ F] layer	—	0.054	—	6.43	36
K ₁₀ B ₁₃ O ₁₅ F ₁₉	<i>R</i> 3 <i>m</i>	B ₁₀ O ₁₂ F ₁ 3 and B ₃ O ₃ F ₆	[B ₁₀ O ₁₂ F ₁₃] and [B ₃ O ₃ F ₆] cluster	—	0.030	—	7.64	37
Rb ₁₀ B ₁₃ O ₁₅ F ₁₉	<i>R</i> 3 <i>m</i>	B ₁₀ O ₁₂ F ₁ 3 and B ₃ O ₃ F ₆	[B ₁₀ O ₁₂ F ₁₃] and [B ₃ O ₃ F ₆] cluster	—	0.030	—	7.32	37

Table S5. Bond valence analysis of RbB₃O₄F₂.

Atom	O1	O2	O3	O4	F1	F2	Σcation
Rb1	0.088	0.124	0.147	0.098	0.354	0.241	1.052
B1	1.027	0.979	1.033	—	—	—	3.039
B2	0.950	0.995	—	1.082	—	—	3.027
B3	—	—	0.780	0.834	0.715	0.731	3.060
Σanion	2.065	2.098	1.960	2.014	1.069	0.972	

The bond valence was calculated by the equation: $S = \exp((R_0 - R)/b)^{38}$ where where S is the experimental bond valence, R the observed bond length, and R_0 and b are fitted bond valence parameters. R_0 of Rb-O, Rb-F, B-O and B-F are 2.263, 2.16, 1.371 and 1.281, $b = 0.37$.

Table S6. Bonding electron density difference ($\Delta\rho$) and contribution percent w (%) of different units in $\text{RbB}_3\text{O}_4\text{F}_2$ calculated by the REDA method.

Units	$\Delta\rho$ (x 10 ⁴)	w (%)
$[\text{BO}_3]^{3-}$	196.39	95.4
$[\text{BO}_2\text{F}_2]^{3-}$	6.96	3.4
$[\text{RbO}_4\text{F}_7]^{14-}$	2.56	1.2

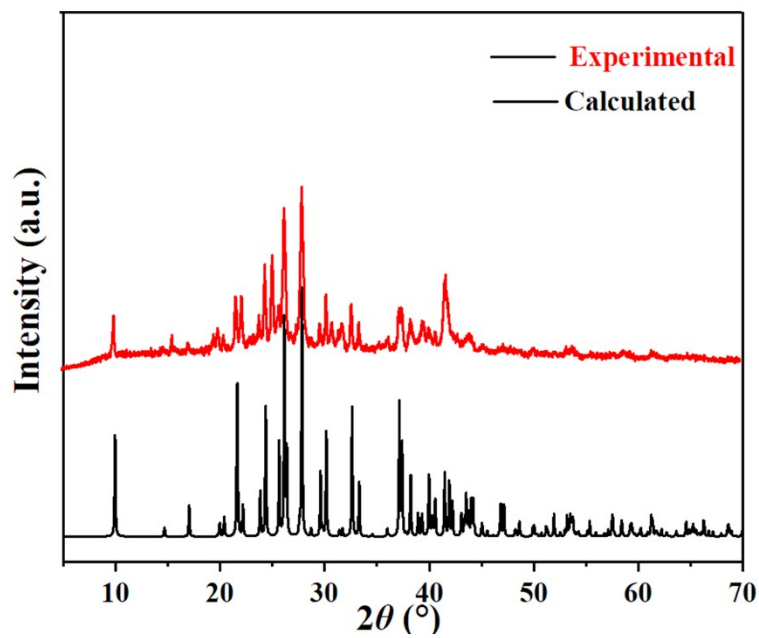


Fig. S1 Calculated and experimental XRD patterns for $\text{RbB}_3\text{O}_4\text{F}_2$. The black curve is the calculated one obtained from single-crystal X-ray structure analysis, the red one is the experimental one for pure phase.

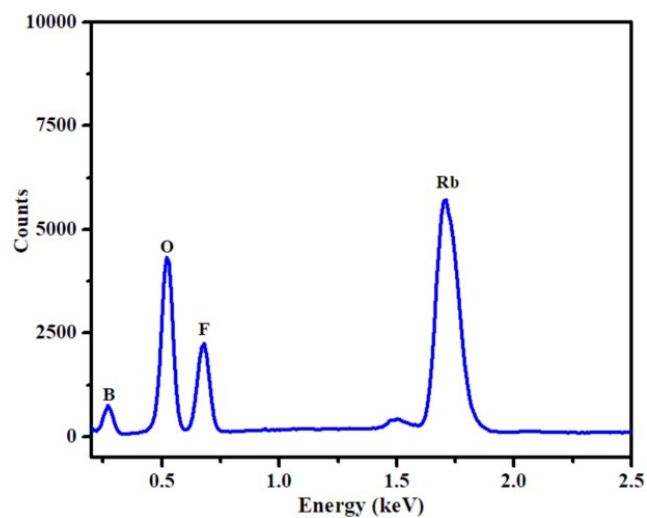


Fig. S2 EDX analysis of $\text{RbB}_3\text{O}_4\text{F}_2$.

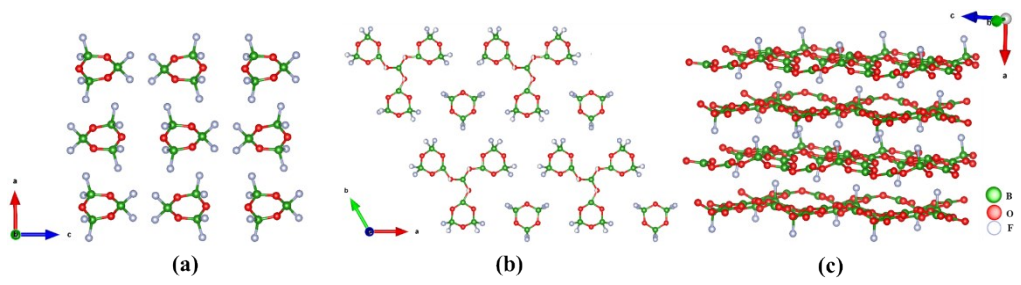


Fig. S3 (a) Isolated $[B_3O_3F_6]^{3-}$ clusters in $Rb_3B_3O_3F_6$. (b) Isolated $[B_{10}O_{12}F_{13}]^{7-}$ & $[B_3O_3F_6]^{3-}$ clusters in $Rb_{10}B_{13}O_{15}F_{19}$. (c) 2D $[B_4O_8F]^{5-}$ layers in RbB_4O_6F .

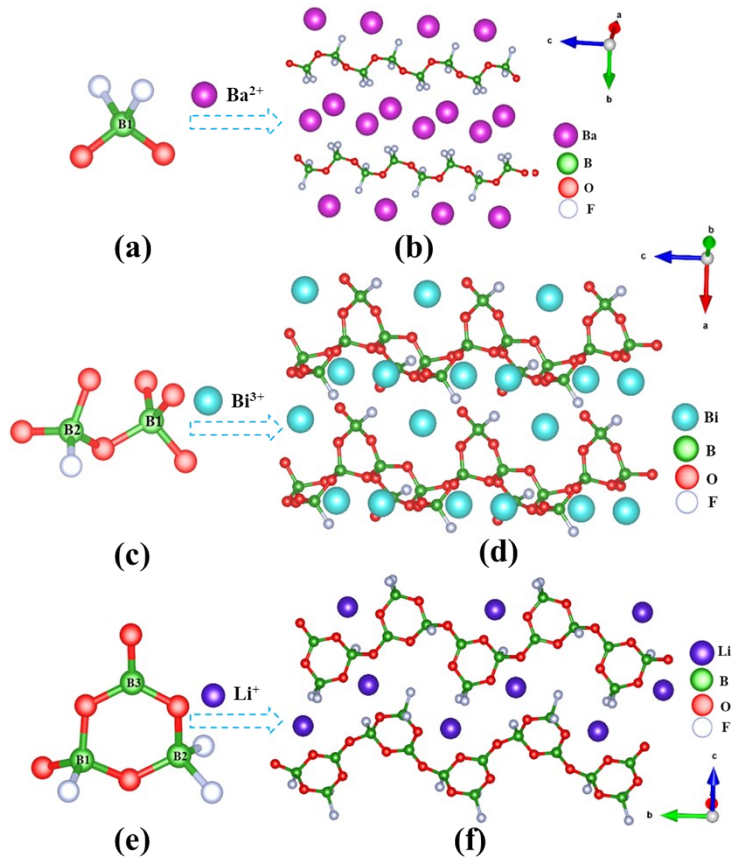


Fig. S4 (a) $[\text{BO}_2\text{F}_2]^{3-}$ FBB of BaBOF_3 . (b) $[\text{BOF}_2]^{-}$ chains of BaBOF_3 . (c) $[\text{B}_2\text{O}_6\text{F}]^{7-}$ FBB of $\text{BiB}_2\text{O}_4\text{F}$. (d) $[\text{B}_2\text{O}_4\text{F}]^{3-}$ chains of $\text{BiB}_2\text{O}_4\text{F}$. (e) $[\text{B}_3\text{O}_5\text{F}_3]^{4-}$ FBB of $\text{Li}_2\text{B}_3\text{O}_4\text{F}_3$. (f) $[\text{B}_3\text{O}_4\text{F}_3]^{2-}$ chains of $\text{Li}_2\text{B}_3\text{O}_4\text{F}_3$.

References

- 1 V. Milman, K. Refson, S. J. Clark, C. J. Pickard and M. D. Segall, *J. Mol. Struct.*, 2010, **954**, 22.
- 2 A. Matveev, M. Staufer, M. Mayer and N. RSch, *Int. J. Quantum Chem.*, 1999, **75**, 863.
- 3 J. P. Perdew, K. Burke and Y. Wang, *Phys. Rev. B*, 1996, **54**, 16533.
- 4 P. Deak, B. Aradi, T. Frauenheim, E. Janzén and A. Gali, *Phys. Rev. B*, 2010, **81**, 153203.
- 5 N. M. Nawi, M. R. Ransing and R. S. Ransing, in *Sixth International Conference on Intelligent Systems Design and Applications*, 2006, 35. 152.
- 6 B. H. Lei, Z. H. Yang and S. L. Pan, *Chem. Commun.*, 2017, **53**, 2818.
- 7 D. Q. Jiang, Y. Wang, H. Li, Z. H. Yang and S. L. Pan, *Dalton Trans.*, 2018, **47**, 5157.
- 8 C. M. Huang, F. F. Zhang, H. Y. Li, Z. H. Yang, H. W. Yu and S. L. Pan, *Chem Eur. J.*, 2019, **25**, 6693.
- 9 (a) Y. Wang, T. Yang, L. Kang, Z. Y. Zhou, R. H. Cong and Z. S. Lin, *Inorg. Chem. Front.*, 2015, **46**, 170; (b) P. Villars, K. Cenzual, J. Daams, R. Gladyshevskii, O. Shcherban, V. Dubenskyy, V. Kuprysyuk and I. Savysyuk, *Landolt Börnstein Group III Condensed Matter*, 2010, **4**, 186.
- 10 (a) S. G. Jantz, M. Dialer, L. Bayarjargal, B. Winkler, L. van Wüllen, F. Pielenhofer, J. Brögch, R. Weihrich and H. A. Höppe, *Adv. Opt. Mater.*, 2018, **6**, 1800497; (b) M. Luo, F. Liang, Y. X. Song, D. Zhao, N. Ye and Z. S. Lin, *J. Am. Chem. Soc.*, 2018, **140**, 6814.
- 11 D. Q. Jiang, G. P. Han, Y. Wang, H. Li, Z. H. Yang and S. L. Pan, *Inorg. Chem.*, 2019, **58**, 3596.
- 12 T. Pilz, H. Nuss and M. Jansen, *J. Solid State Chem.*, 2012, **186**, 104.
- 13 G. Cakmak, T. Pilz and M. Jansen, *Z. Anorg. Allg. Chem.*, 2012, **638**, 1411.
- 14 I. G. Ryss and L. P. Bogdanova, *Russ. J. Inorg. Chem.*, 1959, **4**, 831.
- 15 W. Y. Zhang, Z. L. Wei, Z. H. Yang and S. L. Pan, *Inorg. Chem.*, 2019, **58**, 13411.
- 16 Z. Z. Zhang, Y. Wang, B. B. Zhang, Z. H. Yang and S. L. Pan, *Angew. Chem. Int. Ed.*, 2018, **57**, 6577.
- 17 Y. Wang, B. B. Zhang, Z. H. Yang and S. L. Pan, *Angew. Chem. Int. Ed.*, 2018, **57**, 2150.
- 18 X. F. Wang, Y. Wang, B. B. Zhang, F. F. Zhang, Z. H. Yang and S. L. Pan, *Angew. Chem. Int. Ed.*, 2017, **56**, 14119.
- 19 G. Q. Shi, Y. Wang, F. F. Zhang, B. B. Zhang, Z. H. Yang, X. L. Hou, S. L. Pan and K. R. Poeppelmeier, *J. Am. Chem. Soc.*, 2017, **139**, 10645.
- 20 Z. Z. Zhong, W. Ying, Z. B. Bing, Y. Z. Hua and P. S. Lie, *Chem. Eur. J.*, 2018, **24**, 11267.
- 21 C. Tao and R. Li, *Chem. Eur. J.*, 2020, **26**, 3709.
- 22 M. Q. Gai, Y. Wang, T. H. Tong, L. Y. Wang, Z. H. Yang, X. Zhou and S. L. Pan, *Chem. Commun.*, 2020, **56**, 3301.
- 23 (a) Z. Z. Zhang, Y. Wang, B. B. Zhang, Z. H. Yang and S. L. Pan, *Inorg.*

- Chem.*, 2018, **57**, 4820; (b) M. Luo, F. Liang, Y. X. Song, D. Zhao, F. Xu, N. Ye and Z. S. Lin, *J. Am. Chem. Soc.*, 2018, **140**, 3884.
- 24 M. Mutailipu, M. Zhang, B. B. Zhang, L. Y. Wang, Z. H. Yang, X. Zhou and S. L. Pan, *Angew. Chem. Int. Ed.*, 2018, **57**, 6095.
- 25 S. J. Han, M. Mutailipu, A. Tudi, Z. H. Yang and S. L. Pan, *Chem. Mater.*, 2020, **32**, 2172.
- 26 M. Mutailipu, M. Zhang, B. B. Zhang, Z. H. Yang and S. L. Pan, *Chem. Commun.*, 2018, **54**, 6308.
- 27 C. M. Huang, G. P. Han, H. Y. Li, F. F. Zhang, Z. H. Yang and S. L. Pan, *Dalton Trans.*, 2019, **48**, 6714.
- 28 S. J. Han, Y. Wang, B. B. Zhang, Z. H. Yang and S. L. Pan, *Inorg. Chem.*, 2018, **57**, 873.
- 29 G. Cakmak, J. Nuss and M. Jansen, *Z. Anorg. Allg. Chem.*, 2009, **635**, 631.
- 30 T. Pilz and M. Jansen, *Z. Anorg. Allg. Chem.*, 2011, **637**, 2148.
- 31 G. Q. Shi, F. F. Zhang, B. B. Zhang, D. W. Hou, X. L. Chen, Z. H. Yang and S. L. Pan, *Inorg. Chem.*, 2016, **56**, 344.
- 32 S. J. Han, B. B. Zhang, Z. H. Yang and S. L. Pan, *Chem. Eur. J.*, 2018, **24**, 10022.
- 33 G. P. Han, G. Q. Shi, Y. Wang, B. B. Zhang, S. J. Han, F. F. Zhang, Z. H. Yang and S. L. Pan, *Chem. Eur. J.*, 2018, **24**, 4497.
- 34 C. C. Tang, X. X. Jiang, W. L. Yin, L. J. Liu, M. J. Xia, Q. Huang, G. M. Song, X. Y. Wang, Z. S. Lin and C. T. Chen, *Dalton Trans.*, 2018, **48**, 21.
- 35 Z. Z. Zhang, Y. Wang, H. Y. Li, Z. H. Yang and S. L. Pan, *Inorg. Chem. Front.*, 2019, **6**, 546.
- 36 Y. H. Li, H. Y. Wei, G. P. Han, Z. H. Yang and S. L. Pan, *Chem. Commun.*, 2019, **55**, 8923.
- 37 W. Y. Zhang, Z. L. Wei, Z. H. Yang and S. L. Pan, *Inorg. Chem.*, 2020, **59**, 3274.
- 38 I. D. Brown, *Chem. Rev.*, 2009, **109**, 6858.